

PAPER







Magnetization reversal modes and coercive field dependence on perpendicular magnetic anisotropy in FePt thin films

To cite this article: A Román *et al* 2023 *J. Phys. D: Appl. Phys.* xxxxxx

View the [article online](#) for updates and enhancements.

Proof

Magnetization reversal modes and coercive field dependence on perpendicular magnetic anisotropy in FePt thin films

A Román^{1,*} , A Lopez Pedroso¹ , K Bouzehouane², J E Gómez^{3,4}, A Butera^{3,4} , M H Aguirre^{5,6,7} , M Medeiros Soares^{8,9} , C Garcia¹⁰  and L B Steren¹ 

¹ Instituto de Nanociencia y Nanotecnología CNEA-CONICET—Nodo Constituyentes, Av. Gral. Paz 1499, 1650 San Martín, Pcia. de Buenos Aires, Argentina

² Unité Mixte de Physique CNRS, Thales, Université Paris-Saclay, 91767 Palaiseau, France

³ Instituto de Nanociencia y Nanotecnología, CNEA—CONICET, Nodo Bariloche, Av. Bustillo 9500, 8400 San Carlos de Bariloche, Río Negro, Argentina

⁴ Laboratorio de Resonancias Magnéticas, Gerencia de Física (GF), Centro Atómico Bariloche, CNEA & Instituto Balseiro Universidad Nacional de Cuyo, Av. Bustillo 9500, 8400 San Carlos de Bariloche, Río Negro, Argentina

⁵ Instituto de Nanociencia y Materiales de Aragón, INMA-CSIC-Universidad de Zaragoza, E-50018 Zaragoza, Spain

⁶ Departamento de Física de la Materia Condensada, Universidad de Zaragoza, E-50009 Zaragoza, Spain

⁷ Laboratorio de Microscopías Avanzadas, Universidad de Zaragoza, E-50018 Zaragoza, Spain

⁸ Laboratório Nacional de Luz Síncrotron (LNLS), Centro Nacional de Pesquisa em Energia e Materiais (CNPEM), 13083-970 Campinas, São Paulo, Brazil

⁹ Departamento de Física, Universidade Federal da Paraíba, 58051-900 João Pessoa, Brazil

¹⁰ Departamento de Física and Centro Científico Tecnológico de Valparaíso-CCTVal, Universidad Técnica Federico Santa María, Av. España 1680, Valparaíso, Chile

E-mail: augusto.jre@gmail.com

Received 9 March 2023, revised 25 May 2023

Accepted for publication 9 June 2023

Published xxxxc



CrossMark

Abstract

The competition between shape and perpendicular magnetic anisotropies in magnetic thin films gives rise to unusual magnetic behaviors. In ferromagnetic thin films, the presence of an out-of-plane component of the magnetic anisotropy may induce a transition from planar to stripe-like magnetic domains above a critical thickness, t_c . In this article, we present a detailed study of the magnetization switching mechanism in FePt thin films, where this phenomenon is observed. Using micromagnetic simulations and experiments, we found that below t_c the reversal mechanism is well described by the two-phase model while above this thickness the magnetization within each stripe reverses by coherent rotation. We also analyzed the out-of-plane component of the magnetic anisotropy and its temperature dependence, probing that substrate-induced strains are responsible for the abnormal coercive field behavior observed for FePt films with $t > t_c$.

* Author to whom any correspondence should be addressed.

Supplementary material for this article is available [online](#)

Keywords: magnetic films, magnetic anisotropy, magnetic domains

(Some figures may appear in colour only in the online journal)

1. Introduction

The magnetization reversal mechanisms in thin films have been intensively studied in recent years due to its implications for understanding hysteresis loops and technological applications [1]. The use of magnetic components in random access memories, for example, requires that they show fast and replicable magnetization switching [2]. Therefore, the analysis of the reversal magnetization mechanisms and the possibility of controlling them are an essential input for the evaluation and design of magnetic materials for information storage [2–4].

Controlling magnetic domains presents an exciting opportunity for advancing technology based on domain propagation, including logic circuits, racetrack memories, sensors, and RF devices [5, 6]. The unique properties of stripe domains make them particularly promising for manipulating different magnetic textures, including vortexes, skyrmions, and bubble domains. Recent research has demonstrated that the geometry and local asymmetries in the stripe domain configuration can enable a controlled propagation of skyrmions or bubbles [7, 8]. Moreover, recent investigations show the possibility of controlling the transmission of spin waves using striped domains [9, 10]. Magnetic films with stripe-domain configuration offer diverse applications in new technologies, from optical devices [11] to sensors and storage devices [5].

The structure of magnetic domains in ferromagnetic thin films is strongly influenced by the quality factor ($Q = \frac{K_{\text{PMA}}}{2\pi M_S^2}$), which represents the competition between perpendicular magnetic anisotropy (K_{PMA}) and shape anisotropy ($2\pi M_S^2$), where M_S is the saturation magnetization. When $Q \ll 1$, the magnetic domains are confined to the plane of the film due to the dominance of shape anisotropy. On the other hand, when $Q > 1$, the effective easy axis aligns perpendicular to the film plane, and the domains align accordingly. Bubble and strong stripe structures are characteristic of this regime. Moreover, there are systems with $Q < 1$ where the easy axis lies within the film plane, but the magnetization may exhibit an out-of-plane component depending on the film thickness. Above a critical thickness, t_c , the out-of-plane magnetization component forms periodic stripes with a sine-like profile. However, below t_c , the magnetization remains confined to the film plane. The striped-domain configuration observed in these systems is termed ‘weak stripes’ to differentiate it from the striped-domain configuration observed for $Q > 1$, where stripes appear even at extremely low thicknesses, featuring sharp transitions between oppositely magnetized stripes [5].

The weak stripe domain configuration has been observed in a wide variety of thin films, e.g. $\text{Ni}_{80}\text{Fe}_{20}$ [12, 13], $\text{Fe}_{1-x}\text{Ga}_x$ [14], Fe-N [5, 15] and FePt [16–18] thin films. In these compounds, the PMA and, consequently, the critical thickness has been tuned by changing substrates or adjusting the alloy concentration [19].

Epitaxial FePt thin films have been extensively investigated for perpendicular magnetic recording media applications due to their high perpendicular magnetic anisotropy [20, 21]. The crystal structure of bulk and epitaxial FePt thin films is a chemically ordered body-centered tetragonal cell ($L1_0$) [22–26] at room temperature. This structure can also be described using a face-centered tetragonal (fct) pseudo-cell for which the following lattice parameters have been reported: $a_{\text{FePt}} = 3.852 \text{ \AA}$ and $c_{\text{FePt}} = 3.713 \text{ \AA}$. The tetragonality of this pseudo-cell is $\frac{c}{a} = 0.964$ [22, 27, 28].

In thin films, the formation of the $L1_0$ phase requires high temperatures ($>400 \text{ }^\circ\text{C}$) during the fabrication process or post-deposition treatments, which lead to large grains unsuitable for magnetic recording [21, 29]. Films deposited at room temperature generally form disordered alloys crystallizing in the A1 fcc crystalline structure with small grain sizes [18]. The reported out of plane component of the anisotropy (K_{PMA}) in these films is $\sim 1 \frac{\text{Merg}}{\text{cm}^3}$, almost two orders of magnitude smaller than that of the ordered FePt films [17]. A1 FePt thin films present a transition between in-plane domains to stripe-like domains that occurs at a critical thickness $t_c \approx 30 \text{ nm}$ [17]. Guzmán and co-workers [17] analyzed the temperature dependence of the magnetization of A1 FePt films and reported an abnormal behavior of the coercivity. The authors associated this behavior with a transition from stripe-type to in-plane domains.

The mechanism of magnetization reversal in FePt films is still a matter of controversy. This article presents experiments and micromagnetic simulations to deepen the understanding of the magnetic configuration of $Q < 1$ thin films and their magnetization reversal processes. We will also discuss the magnetization loop parameters, particularly analyzing the correlation between coercive field, system anisotropies, and crystalline structure. This analysis will help to explain the anomalous dependence of coercivity on temperature in this system.

2. Magnetization reversal models

The analysis of the magnetization reversal will be performed in the frame of three models: (I) Coherent rotation, (II) domain wall motion, and (III) the two-phase model. The first two models represent extreme cases of switching behavior, while the third one results from the combination of the first two cases [1, 30]. The angular dependence of the coercivity (ADC) has a characteristic behavior in each model. The ADC is thus an excellent probe for analyzing the magnetization reversal mechanisms in magnetic materials [31].

Stoner and Wohlfarth [32] developed the coherent rotation model for a single domain particle with uniaxial anisotropy. S-W provides also a good description of the magnetization

switching by rotation in thin films [30]. The ADC in the S-W model is given by:

$$H_C(\varphi) = H_0 \begin{cases} \frac{1}{\left(\cos(\varphi)^{\frac{2}{3}} + \sin(\varphi)^{\frac{2}{3}}\right)^{\frac{3}{2}}}, & 0 < \varphi \leq \frac{\pi}{4} \\ \frac{\sin(2\varphi)}{2}, & \frac{\pi}{4} \leq \varphi \leq \frac{\pi}{2} \end{cases} \quad (1)$$

where φ is the angle between the direction of the applied field and the easy axis and H_0 is the coercive field when the magnetic field is applied along the easy axis.

The Kondorsky formula (equation (2)) predicts the ADC of the magnetization reversal mechanism by domain wall motion [33]. In his model, the author assumes that the magnetization reverses once the Zeeman energy exceeds the energy of the domain walls. This mechanism has been observed in many magnetic thin films [34–37]

$$H_C(\varphi) = \frac{H_0}{\cos(\varphi)}. \quad (2)$$

Suponev *et al* [38] generalized the Kondorsky model, proposing a two-phase model. This model assumes that there are only two types of magnetic domains, e.g. two phases. The magnetization of the whole system reverses either by coherent rotation or domain wall movement depending on the magnetic field range. In [38], the ADC for an ellipsoid of revolution with a uniaxial anisotropy along the y axis is thus deduced:

$$H_C(\varphi) = \frac{H_0 \cos(\varphi)}{\frac{1}{y} \sin^2(\varphi) + \cos^2(\varphi)}, y = \frac{N_A + N_x}{N_y} \quad (3)$$

N_x , N_y , and N_z are the demagnetizing factors of the ellipsoid along its main axes, being $N_x = N_z$. N_A is an effective demagnetizing factor that takes into account the contributions of anisotropies other than shape anisotropy favoring an y easy-axis. For an infinite thin film, the demagnetizing factor along the in-plane axes should be $N_x = N_y = 0$, which makes $y \rightarrow \infty$ and, as a consequence, reduces the expression to the Kondorsky formula (equation (2)).

3. Experimental

We studied the magnetism of a series of FePt thin films fabricated by dc magnetron sputtering on naturally oxidized Si (100) substrates. The chamber was pumped down to a base pressure of 1×10^{-6} Torr, and the films were sputtered at 2.6 mTorr of Ar pressure. A power of 20 W, and a target-substrate distance of about 10 cm were used. The sputtering rate was $0.19 \frac{\text{nm}}{\text{s}}$ for the FePt deposition. A 4 nm thick Ru layer capped the samples to prevent oxidation.

The film thickness t was varied from 10 nm to 60 nm and checked by x-ray reflectometry. High-resolution synchrotron x-ray diffraction (XRD) experiments were performed on the XRD2 beamline ($E = 7.00375$ keV) at the Laboratório Nacional de Luz Síncrotron (Campinas, Brazil) using different geometries to collect diffraction patterns. The stacking, interfaces, and crystallinity of the films were analyzed by high-resolution scanning transmission electron microscopy

(HRSTEM). High resolution transmission electron microscopy performed by FEI Tital 80–300 keV image corrected.

The magnetic characterization of the samples was made by measuring magnetization loops using a vibrating sample magnetometer (VSM) and by magnetic force microscopy (MFM) to image magnetic domains at the nanoscale. For the VSM measurements, we applied an external magnetic field in the plane of the films, varying the angle between the applied field and the Si[100] direction in the range $0^\circ < \varphi < 180^\circ$. The magnetization loops were measured between 50 K and 300 K. MFM images were recorded by an Asylum AFM, using the phase detection mode at 77 K and 300 K. We used Asylum High Coercive HC5SP3 ($H_c \approx 5000$ Oe) tips for the measurements. MFM images of remanent states were measured after saturating the films with a magnetic field of $H \sim 6000$ Oe applied in the film's plane.

Micromagnetic simulations using Mumax3 open source software [39–42] were performed to evaluate the magnetic configurations and their dependence with magnetic field. The simulations were made keeping fixed the saturation magnetization, $M_S = 1130 \frac{\text{emu}}{\text{cm}^3}$ and the exchange stiffness constant $A_{\text{ex}} = 9.5 \times 10^{-7} \frac{\text{erg}}{\text{cm}}$ [43, 44]. To simulate the grains of the film, we defined regions through the Voronoi Tessellation and reduced the exchange interaction between grains, varying its value to reproduce the experimental remanence and coercive field. The perpendicular magnetic anisotropy constant K_{PMA} was varied between $0.7 \frac{\text{Merg}}{\text{cm}^3}$ and $1.8 \frac{\text{Merg}}{\text{cm}^3}$. The calculations were performed at zero temperature. Simulated and experimental results obtained at room temperature are expected to be similar, since the Curie temperature of A1 FePt films is around 580 K [45].

4. Results and discussion

4.1. FePt films structural analysis

We investigated the FePt films crystalline structure by HRSTEM and XRD. The cross-section of a 40 nm FePt film measured by HRSTEM, shown in figure 1(a), puts in evidence the polycrystalline structure of the samples. The films are formed by grains that present different degrees of crystalline order, e.g. white circles indicate the regions with highly ordered structure. HRSTEM images also served us to get a description of the film stacking. Films are composed of small grains of a few nanometers (3–4 nm) at the first layers from the substrate, acquiring a columnar profile with a width of tens of nanometers beyond the interface zone. The average grain size of the sample of 40 nm FePt thickness is 11.3 ± 0.4 nm, where the average was calculated including grains and columns widths.

Figure 1 also shows fast Fourier transformed for the calculation of the selected area electron diffraction patterns of different regions of the sample. Patterns presenting only the (111) reflection were found in some zones of the films and were associated with the A1 disordered phase (figure 1(b)). Other regions presented the (001) reflection (figure 1(c)), indicating that there are grains formed in the ordered phase ($L1_0$) [43].

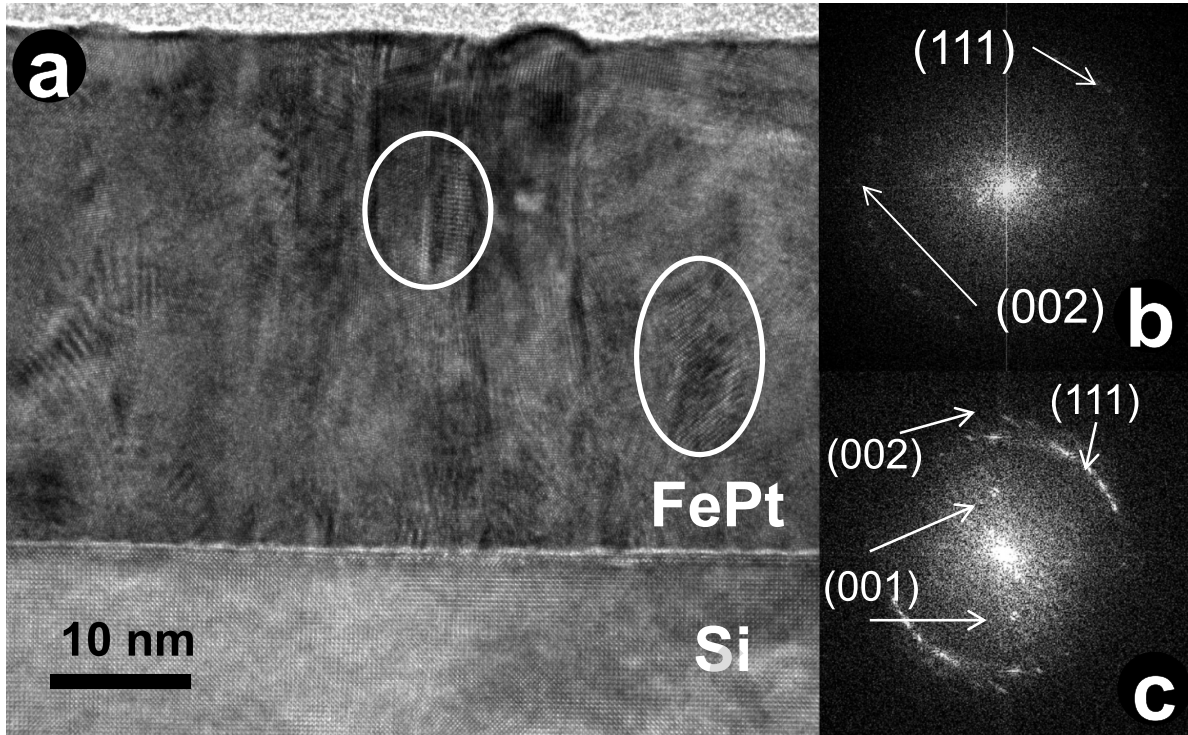


Figure 1. (a) Cross sectional HR-TEM image and (b), (c) SAED pattern from a 40 nm thickness FePt film deposited on a silicon substrate. White circles indicate ordered regions of the sample.

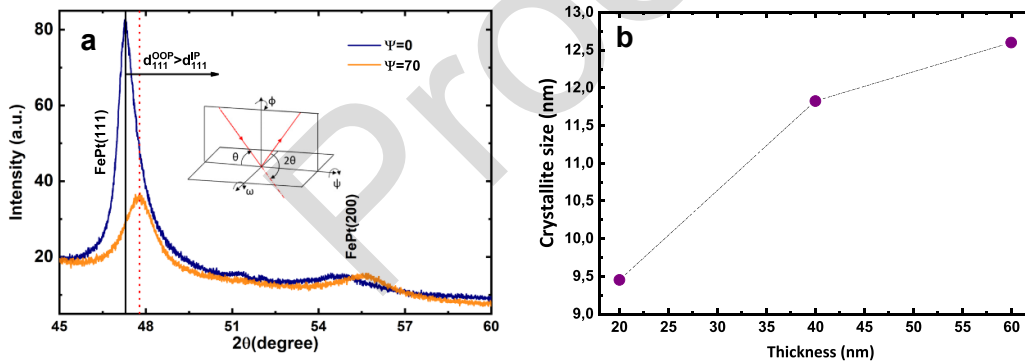


Figure 2. (a) XRD patterns of FePt(60 nm)/Si recorded for $\theta/2\theta$ for $\psi = 0$ and $\psi = 70$. (b) Calculated average crystallite size using the Scherrer equation and the width of the (111) reflection vs the film thickness for FePt on silicon.

In figure 2(a) we show the XRD pattern for a 60 nm thick FePt film measured using different geometries. On the one hand, we used the conventional $\theta/2\theta$ geometry to measure the distance between crystallographic planes parallel to the substrate surface. On the other hand, we set $\psi = 70^\circ$ (figure 2(a)) in order to measure the distance between planes that are almost perpendicular to the substrate surface [46]. The conventional $\theta/2\theta$ measurement ($\psi = 0^\circ$) indicates that the film presents a (111) texture perpendicular to the film plane. The lattice parameter deduced from the (111) peak is $a = 3.85 \text{ \AA}$ in agreement with previous works [17, 18, 47]. The XRD pattern measured at $\psi = 70^\circ$ presents a shift of the (111) peak to larger angles (figure 2(a)), indicating that the substrate induces an in-plane compression on the film. Equation (4) is an estimation of the film strain along the direction perpendicular to the substrate plane

$$\epsilon = \frac{2\nu}{(1 + \nu) \sin(70^\circ)} \frac{d_{\psi=0} - d_{\psi=70}}{d_{\psi=0}} \times 100\% \quad (4)$$

$d_{\psi=0}$ and $d_{\psi=70}$ are the distances between planes parallel to the films surface and those almost perpendicular to the substrate, respectively and ν is the Poisson's ratio [16, 46, 48]. Using this expression, we obtained a 0.66% strain in the FePt film.

From the (111) XRD peak width, we calculated the average crystallite size of the alloy as a function of the film thickness using the Scherrer formula [49] (figure 2(b)). The crystallite size increases with the film thickness from 9.5 nm to 12.5 nm as expected from the description of the stacking obtained from HRSTEM measurements. Also in the case of the 40 nm FePt sample, the crystallite size measured by XRD (11.8 nm) is in agreement with the value obtained from HRSTEM images.

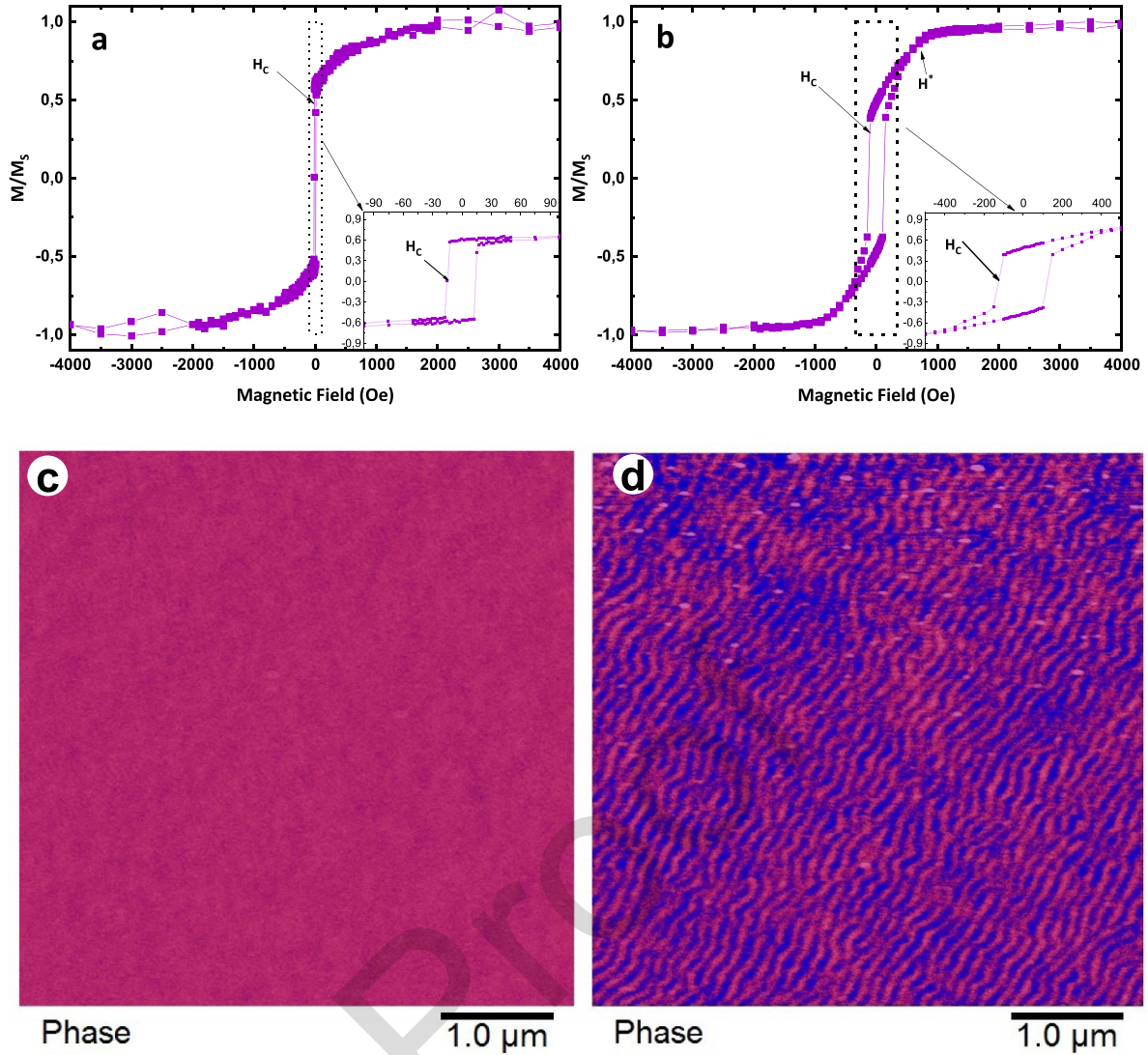


Figure 3. In-plane easy axis ($\varphi = 0^\circ$) hysteresis loops and MFM images for FePt films of (a), (c) $t = 10$ nm and (b), (d) $t = 60$ nm, respectively. All the measurements were performed at $T = 300$ K.

Takahashi and coworkers [50–52] found a strong correlation between the crystalline structure and the grain size of FePt alloys. These authors reported a transition from A1 to L1₀ FePt crystalline structure as the grain size varies from 4 nm to 7 nm providing another evidence of the presence of grains in the ordered phase in our samples

The structural characterization reveals two main facts. Firstly, HRSTEM and XRD results suggest a mix of ordered and disordered FePt phases, where the A1 is the major phase with a small fraction of L1₀ nanograins embedded; secondly, that the structure of the films is compressed in the plane by the substrate.

4.2. Critical thickness t_c

The analysis of the hysteresis loops shows a notable difference in the shape of the curves, depending on the film's thickness (figures 3(a) and (b)). The magnetization curves for thin

FePt films ($t < 30$ nm) present coercive fields smaller than 20 Oe and relatively squared loops (table 1), while thicker films present larger coercive fields and a linear dependence of the magnetization for $-H_c < H < H^*$ (figure 3).

In figures 3(c) and (d), we present the MFM images of the 10 nm and 60 nm samples, taken in remanence after saturating the magnetization of the film. The MFM measurements of films with $t < t_c$ images did not show any magnetic contrast, and no domain walls were detected even for scan sizes up to $20 \times 20 \mu\text{m}^2$. Combining this result with the magnetometry measurements, it can be concluded that the magnetization lies in the plane of the sample and the domains are significantly larger than the MFM scan size. On the other hand, thick films ($t > 30$ nm) show striped magnetic domains with out-of-plane magnetization components (figure 3(d)). These results indicate a change of the domain structure at a critical thickness t_c between 20 and 40 nm. Our measurements agree with previous results [18] that estimated a critical thickness of 30 nm for FePt films deposited on silicon.

Table 1. Remanence ($\frac{M_R}{M_S}$), coercive field (H_C) and stripes domain period (λ) of FePt films of different thickness. Uncertainties are shown in parentheses.

Thickness (nm)	$\frac{M_R}{M_S}$	H_C (Oe)	λ (nm)
10	0.65(0.02)	15(3)	—
20	0.84(0.02)	10(3)	—
40	0.62(0.02)	42(3)	90(10)
49	0.53(0.02)	157(3)	104(10)
60	0.46(0.02)	148(5)	110(10)

Murayama [53] proposed a micromagnetic model to describe the free energy density of a ferromagnetic film with striped domains. The model postulates a uniaxial anisotropy perpendicular to the film's plane, and assuming that the magnetization is constant along the normal to the film axis, the author was able to reduce the dimensionality of the problem to 2D. Based on these assumptions, Murayama derived an expression for the stripe period λ as a function of film thickness t and magnetic parameters:

$$\frac{\lambda}{2} = \sqrt{2\pi t} \sqrt[4]{\frac{A_{\text{ex}}}{2\pi M_S^2} \left(1 + \frac{2\pi M_S^2}{K_{\text{PMA}}}\right)}, \quad (5)$$

where A_{ex} is the exchange stiffness constant, M_S is the saturation magnetization, K_{PMA} is the perpendicular magnetization anisotropy constant and t is the thickness of the film. Replacing the exchange stiffness constant $A_{\text{ex}} = 9.5 \times 10^{-7} \frac{\text{erg}}{\text{cm}}$ and $M_S = 1130 \frac{\text{emu}}{\text{cm}^3}$ from [43] in equation (5), we estimated a perpendicular anisotropy constant of $1.4 \pm 0.5 \frac{\text{Merg}}{\text{cm}^3}$ for films with thickness above t_c . This result agrees with the value obtained from the magnetometry measurements using the area-method [54] and with the values reported in previous studies on disordered FePt films deposited on silicon [17, 18].

4.3. Magnetization reversal mechanism at room temperature

Both the magnetization and the MFM results suggest that the magnetization reversal mechanism should depend on the FePt film thickness, being particularly different for films with $t < t_c$ and $t > t_c$. To analyze the samples' magnetization reversal process, we performed measurements of the angular dependence of the magnetization curves with the magnetic field applied in the plane of the films.

4.3.1. Films with $t < t_c$. The angular dependence of the remanent magnetization for films thinner than t_c reveals the presence of an in-plane uniaxial anisotropy with an easy-axis oriented along the Si[100] direction (figures 4(a) and (b)). The magnetization loops measured with the magnetic field applied parallel, ($\varphi = 0^\circ$) and perpendicular ($\varphi = 90^\circ$) to the easy-axis (e.a) are shown in figure 4(a). A square loop with $H_C = 15$ Oe is observed for loops measured $\varphi = 0^\circ$, while a two-steps loop is observed for $\varphi = 90^\circ$. The easy axis exhibits a remanence of $M_R = 0.65M_S$, which we attribute to the

presence of $L1_0$ grains as observed in the structural characterization. The two-step loop observed when the magnetic field is applied along the hard axis can be attributed to the coexistence of two anisotropies: a uniaxial induced during the fabrication process or the morphology of the substrate and a biaxial induced by the substrate structure [55].

The angular dependence of the coercive field is shown in figure 4(c). As can be seen, the coercive field increases with φ , reaching a maximum value close to $\varphi = 90^\circ$. In the same figure, the experimental data was compared with calculated values arisen from Stoner–Wohlfarth [32], Kondorsky [33], and two-phase models [38]. The two-phase model [38] is the best fit for our experimental data, even though the fact that the coercive field is not zero at the hard axis, as expected for this model. Suponev and coworkers [38] attributed the non-zero $H_C(\varphi = 0^\circ)$ to the grain easy axis distribution due to the polycrystalline nature of the sample.

The fitted value of $y = 6.76$ derived from equation (3) for our FePt films indicates the presence of a considerable perpendicular magnetic anisotropy induced by strain, consistent with previous reports [17]. In thin films, the in-plane demagnetizing factors are zero, so the parameter y should be infinite. However, we attribute the finite value of y to the non-zero effective demagnetizing factors in the plane of the sample due to the presence of an out of plane component of the anisotropy.

4.3.2. Films with $t > t_c$. The magnetization loops for thick films do not depend appreciably on the magnetic field orientation which is expected due to the rotatable anisotropy that characterizes films with stripe-domains [5, 18, 56].

This behavior arises from the stripe-domain structure of these films at remanence. Therefore, complementary experiments and micromagnetic simulations were needed to get an insight into the magnetization reversal mechanisms of these films. MFM measurements were performed under an external magnetic field applied along the direction of the stripes. The MFM images were acquired in a single scan, varying the magnetic field during the measurement. The stripe patterns were observed up to 1000 Oe and disappeared for magnetic fields larger than 2000 Oe (figure 5(a)). However, the stripe period does not depend appreciably on the magnetic field intensity (figure 5(b)).

Micromagnetic simulations of magnetization loops and the domain structure were performed to gain insight. The magnetization loops of 60 nm thick films were reproduced setting a perpendicular magnetic anisotropy constant of $K_{\text{PMA}} = 1.6 \frac{\text{Merg}}{\text{cm}^3}$ and considering an intergrain interaction of 20% of A_{ex} , the interaction between neighboring spins (figure 6). A good agreement between the experimental and the simulated loops is shown in figure 6, except for the region $H_C < H < H^*$, where a difference is observed. The experimental curve suggests that the magnetization of a fraction of the sample requires stronger fields to saturate. Two possible scenarios were analyzed to explain this behavior: the presence of $L1_0$ grains with stronger K_{PMA} and edge effects due to the samples' finite size.

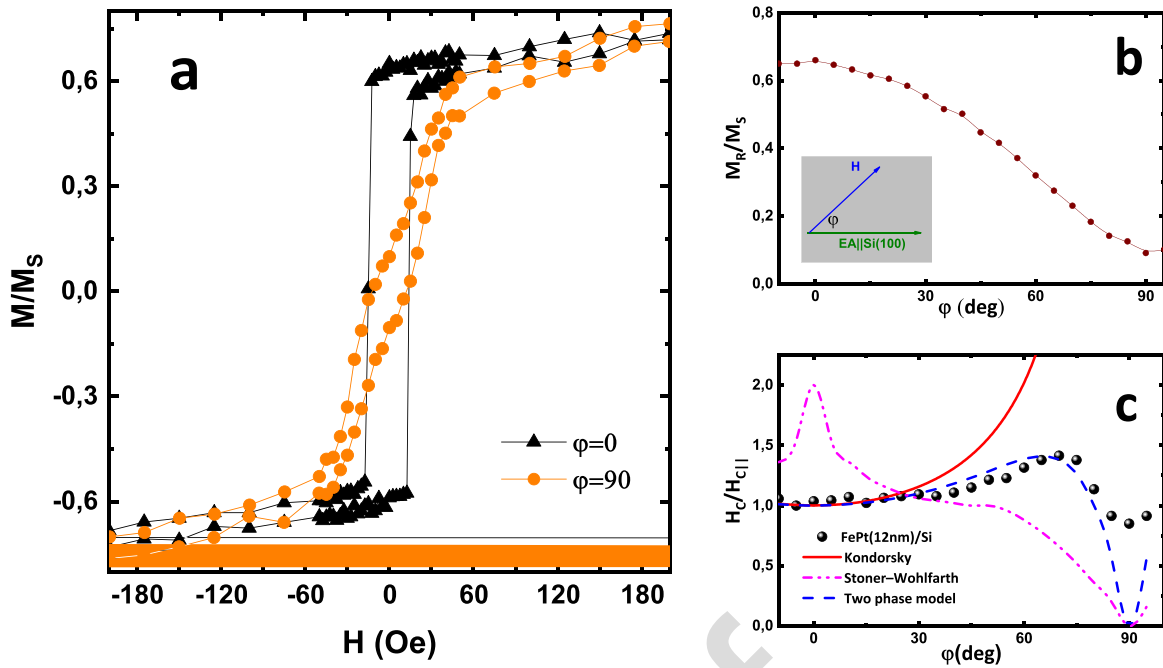


Figure 4. (a) Hysteresis loops measured for $\varphi = 0^\circ$ and $\varphi = 90^\circ$ for FePt(10 nm)/Si. (b) angular dependence of the remanent magnetization. (c) Angular dependence of the coercive field for a 10 nm thickness FePt thin film plotted together with the magnetization reversal models: Stoner–Wohlfarth, Kondorsky and two phase model.

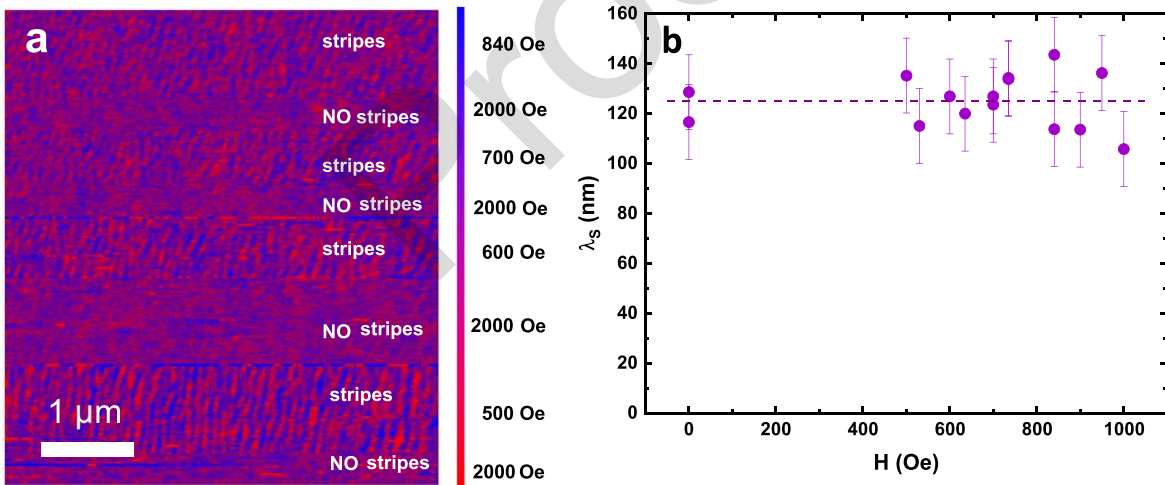


Figure 5. MFM image from a 49 nm thick FePt film with an external magnetic field applied parallel to the stripes, with the different fields being applied during a single scan. (b) The stripe-domain period (λ_s) was calculated from the MFM images as a function of the magnetic field.

The micromagnetic simulations confirmed that the presence of a few percent of $L1_0$ nanometric grains embedded in the films affects the saturation of the magnetization loops. We ruled out sample edge effects due to the macroscopic size of the films.

The value of the anisotropy constant agrees with the one calculated from MFM measurements in section 4.2, and the reduction of the exchange interaction at the grains

boundaries is expected for polycrystalline films [47, 57]. For $H < 1200$ Oe, the cross sections of the simulated magnetic domains in the $x - y$ plane successfully reproduce the stripes observed in MFM images (figure 6). The field dependence of the $x - z$ cross-sections puts in evidence that the magnetization within the stripes reverses by uniform rotation. The magnetic moments at the $y - z$ cross-section arrange to minimize the magnetostatic energy. Closure domains are at surface zones,

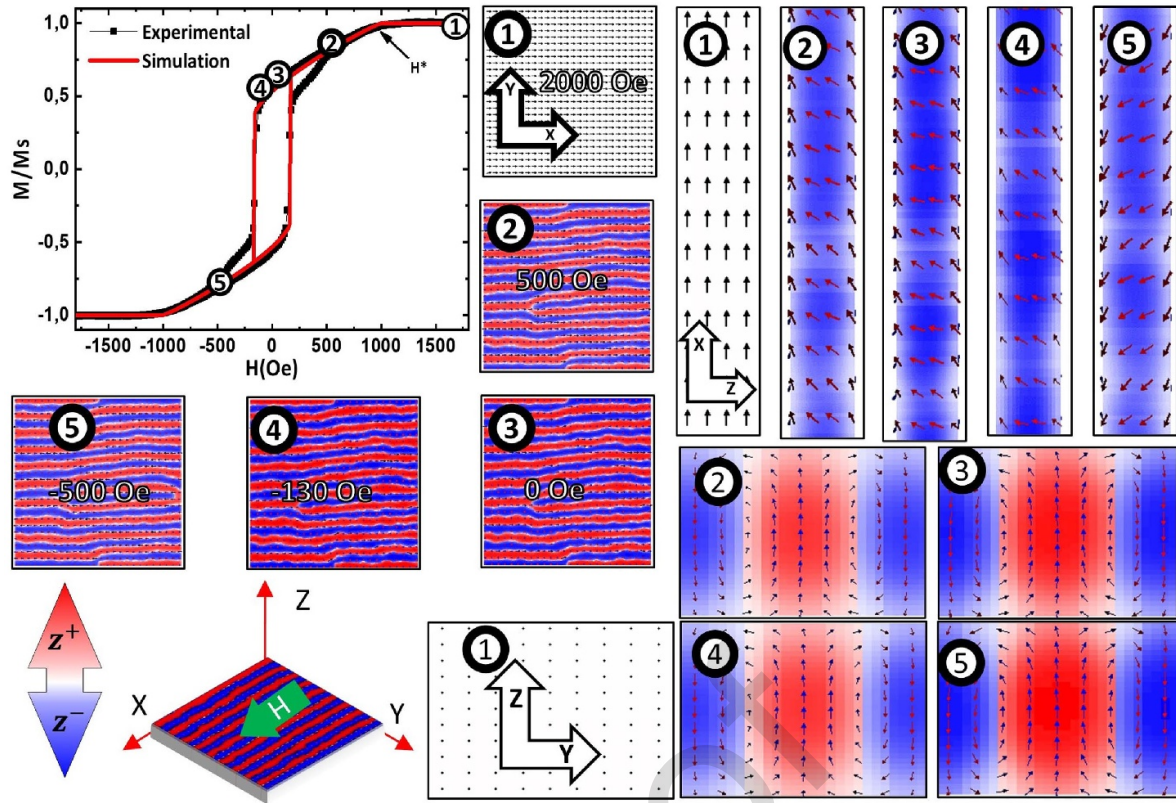


Figure 6. Experimental and simulated hysteresis loops of a FePt 60 nm/Si. (1–5) Domain structure as a function of magnetic field. $x - y$, $x - z$ and $y - z$ crosssections. The $x - z$ crosssection is from the center of a stripe.

while vortex cores along the x -axis are observed at the center of the sample ($z \sim t/2$).

The profile of the m_z (figures 7(a) and (c)) component for the 60 nm thickness simulation varies periodically along the y -axis, with a period $\lambda_s = 90 \pm 10$ nm that does not depend on the magnetic field. However, m_z reaches the maximum at the coercive field e.g. the magnetic moments rotate out of the plane of the film during the magnetization reversal process. The profile of the m_x component (figures 7(b) and (d)) presents a periodic dependence with a period of $\frac{\lambda_s}{2}$. This period is related to the space distribution of the vortex cores. The $m_x(y)$ maximums correspond to the core of the vortices that give stability to the striped domain structure. For magnetic fields smaller than H^* , the amplitude of its oscillations increases as the field decreases until the coercive field (H_c), where m_x reverses.

4.4. Magnetization reversal at low temperatures

The coercivity of the thin films ($t < t_c$) decreases with temperature, as a typical ferromagnet does (figure 8), while the coercive field of thick films ($t > t_c$), instead, presents an abnormal temperature dependence with a maximum located at a characteristic temperature, T^* , which has been reported to be thickness dependent by Guzman and coauthors [17]. In their paper, these authors suggested that at T^* , there could be a transition in the domain configuration, from a striped-type to fully in-plane domains.

In figure 9, we show images measured by MFM at different temperatures for a 49 nm thick FePt film, which has a maximum coercivity at $T = 150$ K [17]. The domain configuration remains striped between 77 K and room temperature despite the variation of the coercive field behavior as a function of temperature. The stripe period of our samples increases an 18% as the temperature decreases from 300 to 77 K. According to equation (5), an increase of the stripes period is associated to a decrease of the quality ratio Q . Therefore, the increase of λ observed in our experiments might indicate a decrease of K_{PMA} as the temperature is lowered.

This temperature dependence of the perpendicular magnetic anisotropy in FePt films is associated to magnetostrictive effects. The difference between film and substrate thermal expansion coefficients may induce strains on the films that would change the perpendicular anisotropy [58, 59]. To evaluate the effect of temperature on the strain of the film, we performed XRD measurements below room temperature. We estimated the in-plane compression of $d(111)$ interplane distances from XRD patterns, measured between 150 K and 300 K. The compression (ϵ) as a function of temperature shown in figure 10 indicates that there is a reduction of the in-plane strain when the temperature decreases. An anisotropy induced by strains was estimated after the XRD results and using known constants for the FePt system. For the calculation of the stress a Poisson's modulus $\nu = 0.33$ and a Young's modulus $E = 180$ GPa of FePt [60] were used. The magnetostriction coefficient reported for FePt films in the disordered

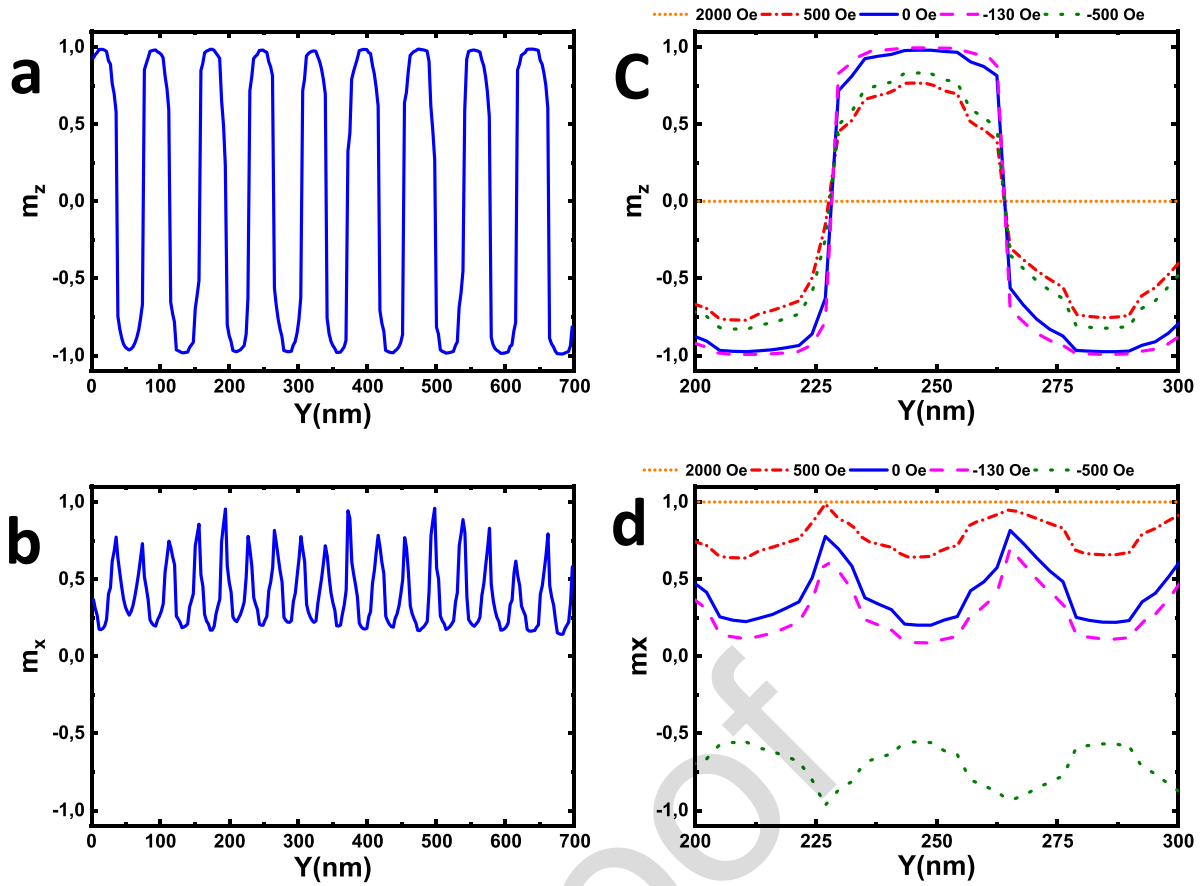


Figure 7. (a) m_z and (b) m_x profile along Y axis for a 60 nm FePt thin film simulated at remanence. Detail of the magnetic field dependence of the (c) m_z and (d) m_x profile.

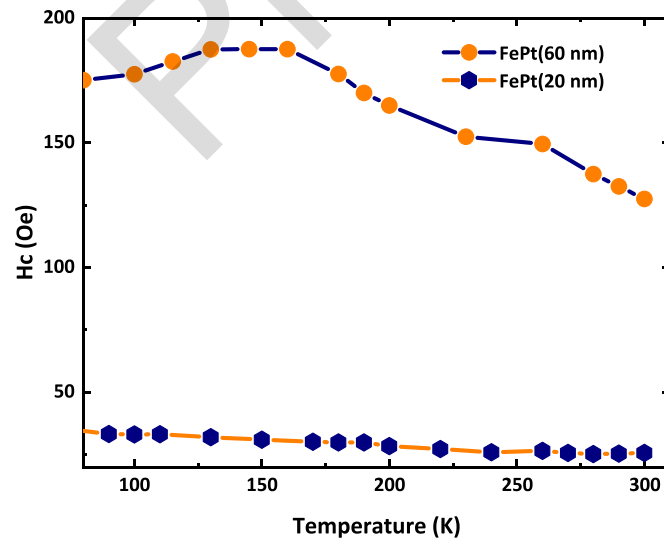


Figure 8. Measured temperature dependence of the coercive field for 60 and 10 nm thickness FePt films.

phase is between 100 ppm and 170 ppm [61, 62]. The variation of the anisotropy was so calculated, finding a change of $\Delta K_{300 \rightarrow 150} = -0.5 \pm 0.1 \frac{\text{Merg}}{\text{cm}^3}$ when decreasing temperature from RT to 150 K.

The influence of a K_{PMA} variation, between $0.7 \frac{\text{Merg}}{\text{cm}^3}$ and $1.8 \frac{\text{Merg}}{\text{cm}^3}$, on the magnetization process was then analyzed

by simulations. Figures 11(a) and (b) shows the remanence and coercive field dependence on K_{PMA} . The remanence decreases monotonically with increasing K_{PMA} while the coercive field presents a maximum at $K_{\text{PMA}} = 1.2 \frac{\text{Merg}}{\text{cm}^3}$. As we show in figures 11(c) and (d), simulated domains are organized in stripes in the whole K_{PMA} range. The stripes

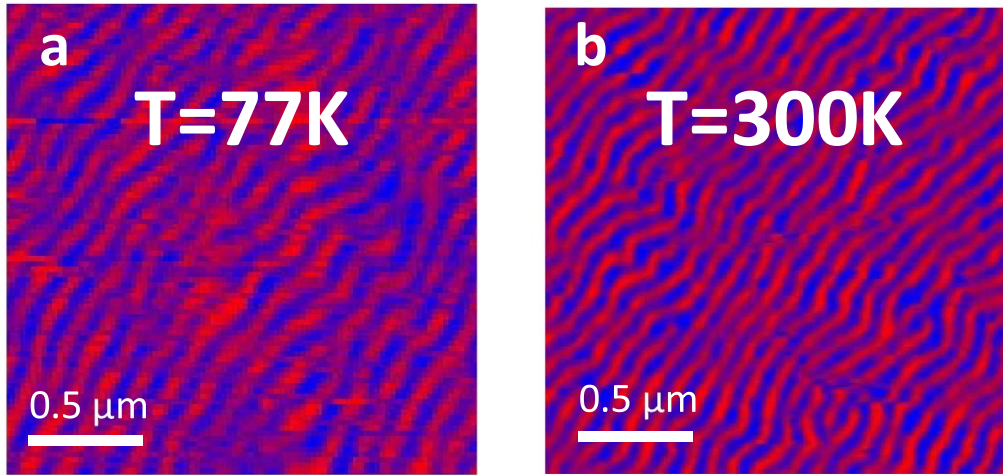


Figure 9. MFM images from a 49 nm thick FePt film measured at (a) $T = 77$ K and (b) $T = 300$ K.

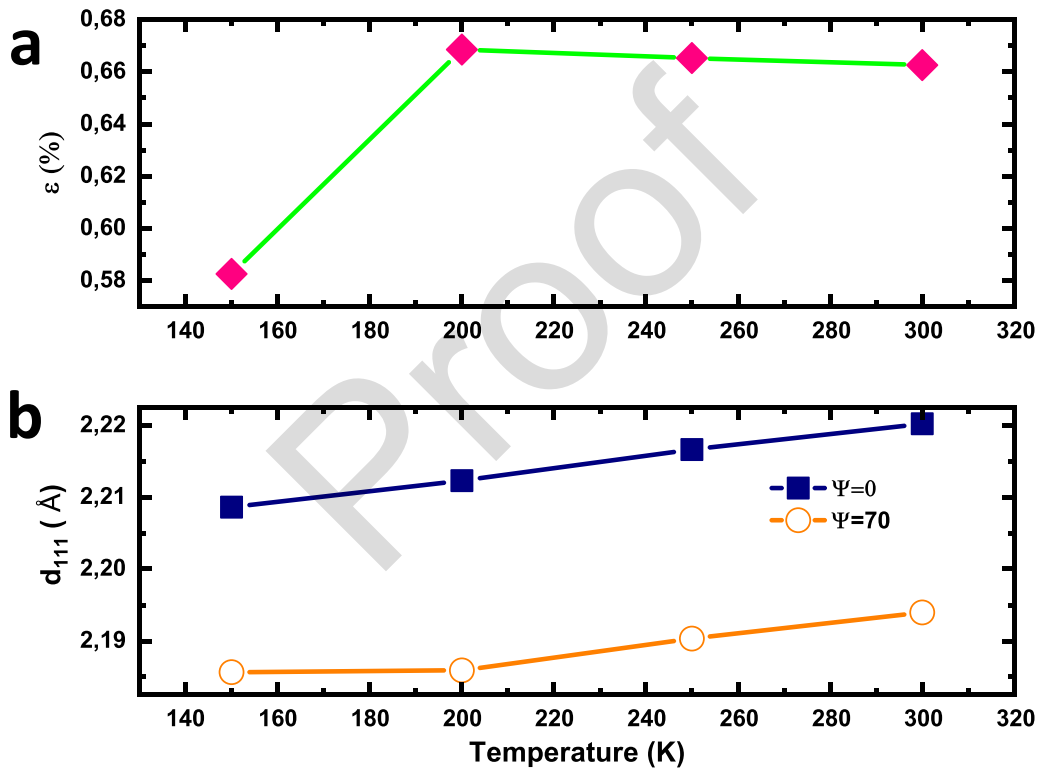


Figure 10. (a) difference between nearly inplane interplannar distance and out of plane interplannar distance. (b) d_{111} temperature dependence for different XRD geometries.

period increases 20% as the anisotropy constant decreases a 60%.

As mentioned above, from the strain analysis as function of temperature, we deduced a change of K_{PMA} from $1.6 \frac{\text{Merg}}{\text{cm}^3}$ at room temperature to $1.1 \frac{\text{Merg}}{\text{cm}^3}$ at 150 K attributed to the temperature variation of the strain. Figure 11 shows that the anisotropy constant value that corresponds to the maximum coercivity is in this anisotropy range. These results provide clear evidence to the fact that the anomalous temperature dependence of the coercive field is a consequence of strain-induced changes of the anisotropy.

In figure 12, we present hysteresis loops calculated for anisotropy values higher and lower than $K_{PMA-MAX} = 1.2 \frac{\text{Merg}}{\text{cm}^3}$, where the maximum coercivity is observed. The loop calculated for $K_{hi} = 1.6 \frac{\text{Merg}}{\text{cm}^3} > K_{PMA-MAX}$ presents a sharp change in the magnetization at the coercive field. In contrast, the one calculated for $K_{lo} = 0.9 \frac{\text{Merg}}{\text{cm}^3} < K_{PMA-MAX}$ exhibits a smooth variation of the magnetization near the coercive field.

In order to understand the difference in the magnetization reversal process of the calculated loops, we simulated the dynamic of the micromagnetic state near the coercive field for both cases. The initial magnetization state ($t = 0$ ns)

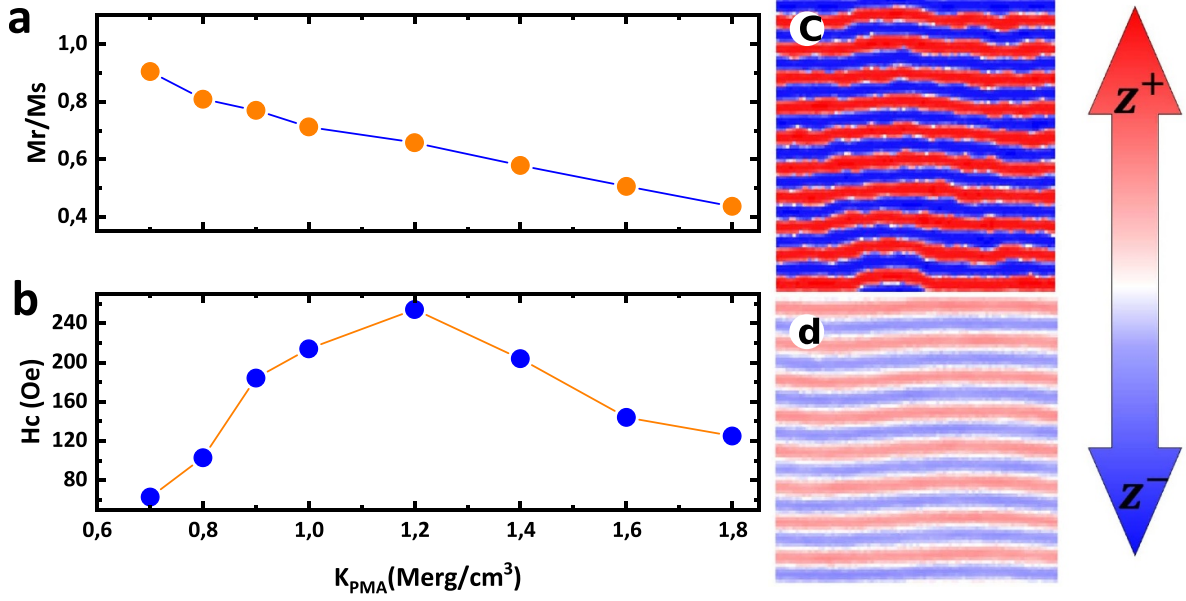


Figure 11. Simulated (a) remanence and (b) coercive field as a function of the magnetic anisotropy constant for a 60 nm FePt film. Simulated magnetic domain configuration for (c) $K_{lo} = 0.9 \frac{\text{Merg}}{\text{cm}^3}$ and (d) $K_{hi} = 1.6 \frac{\text{Merg}}{\text{cm}^3}$.

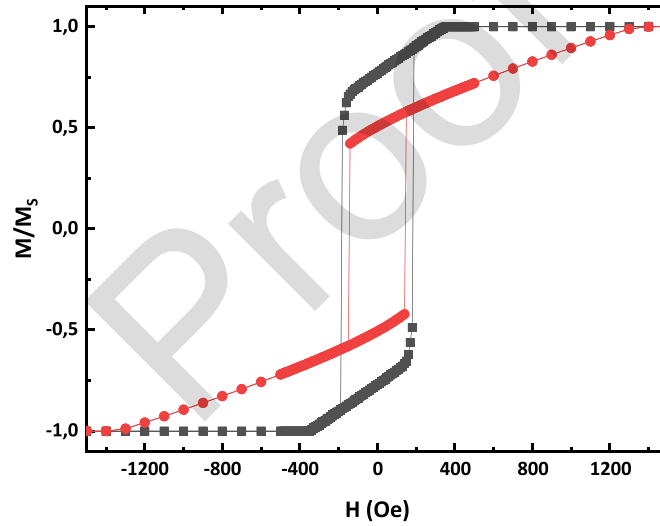


Figure 12. Simulated hysteresis loops from a 60 nm FePt film with (■) $K_{lo} = 0.9 \frac{\text{Merg}}{\text{cm}^3}$ and (●) $K_{hi} = 1.6 \frac{\text{Merg}}{\text{cm}^3}$ perpendicular magnetic anisotropy constant.

was taken to be that of $M(H^* \lesssim H_c)$ calculated for K_{lo} and K_{hi} (figures 13(a) and (e)). At $t > 0$ ns, a magnetic field H^{**} slightly larger than the coercivity was applied to the systems and the temporal evolution of the magnetic state was simulated for K_{lo} (figure 13 top) and K_{hi} (figure 13 bottom). Both H^* and H^{**} were applied along the $-x$ direction.

For K_{lo} , the magnetic moments rotate in the plane of the film. During the first 6 ns, the spins rotate from the x -axis to the y -axis (figures 13(a) and (b)). At $t = 8$ ns, the formation of vortices gave place to the appearance of reversed domains parallel to the applied field (figure 13(c)). Finally, after 10 ns, the formed domains expand from one side of the sample to its center (figure 13(d)). On the other side, For $K_{PMA} > K_{PMA-MAX}$,

the magnetic moments rotate out of the plane of the film. The stripe structure remains throughout the whole magnetization reversal process. There is a coherent rotation of the magnetic moments of each stripe, but the stripes do not rotate simultaneously.

The magnetization reversal process is notably faster for films with K_{hi} . As shown in figure 13, the spins complete their rotation after 8 ns. For films with low anisotropy, we performed the calculations using a time frame of 20 ns, and observed the end of the reversal process at 14 ns. This result almost doubles the time length of the reversal process compared to films with K_{hi} . The simulation results indicate that the abnormal temperature dependence of the coercive field is

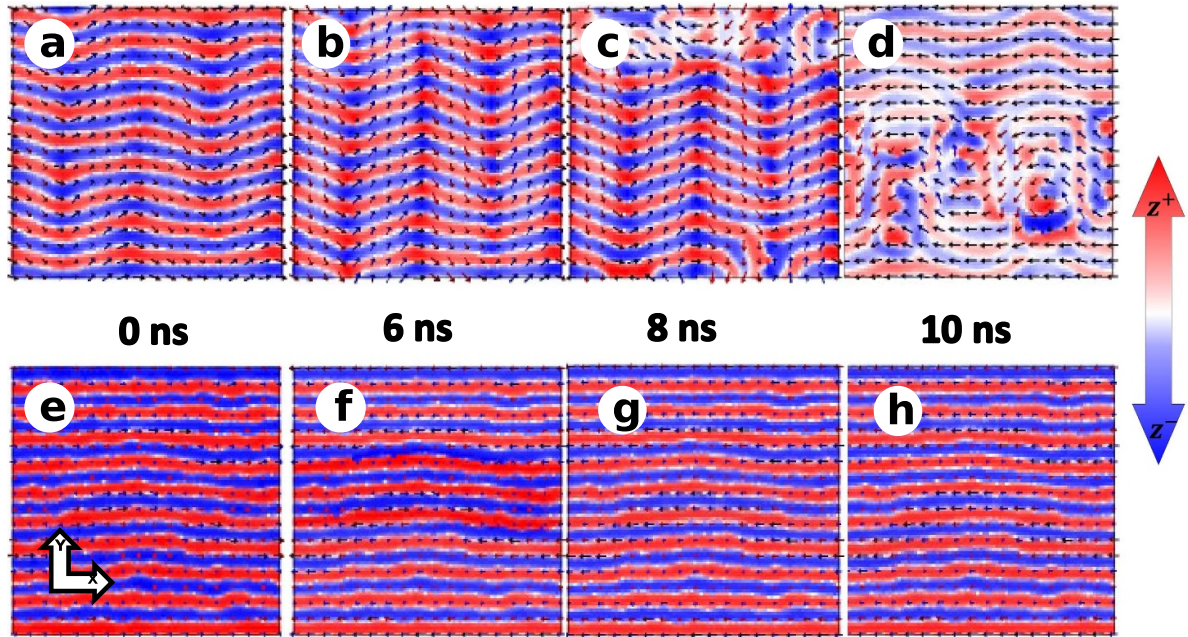


Figure 13. Simulated time evolution of the magnetic domain configuration from a 60 nm FePt film with (a)–(d) $K_{\text{PMA}} = 0.9 \frac{\text{Merg}}{\text{cm}^3}$ and (e)–(h) $K_{\text{PMA}} = 1.6 \frac{\text{Merg}}{\text{cm}^3}$. The initial magnetization state ($t = 0$ ns) was taken to be that of $M(H^* \lesssim H_c)$. A magnetic field $H^{**} > H_c$ in the negative x -direction was applied during the time evolution.

related to a variation of the perpendicular magnetic anisotropy induced by the mismatch between thermal expansion coefficients of films and substrate, inducing a change of the magnetization reversal process.

The existence of a magnetic anisotropy constant value where the coercivity reaches a maximum ($K_{\text{PMA-MAX}}$) was also observed in simulations of FePt films with thicknesses between 30 nm and 60 nm. Guzmán and co-workers [17] report that when the thickness of the film decreases, the maximum in coercivity occurs at temperatures closer to room temperature. In agreement with this result, we observed that as the thickness of the simulated film decreases, the value of $K_{\text{PMA-MAX}}$ increases. Also, a maximum in the thickness dependence of the coercivity was observed, in agreement with the results published by Sallica and co-workers [18].

5. Conclusions

We have performed a detailed study of the magnetization reversal mechanisms in FePt films that present a transition from planar to stripe-like magnetic domains above a critical thickness t_c due to the presence of an out of plane component of the magnetic anisotropy. At room temperature, the reversal mechanism of the thinner films ($t < t_c$) was described by the two-phase model that combines coherent rotation with domain-wall movement. In contrast, the striped domain configuration, observed at remanence, dominates the magnetization reversal process in thicker films ($t > t_c$). In this regime each stripe domain reverses by coherent rotation. Moreover, we succeeded in explaining the origin of the anomalous temperature variation of the coercive field observed in thick films. The effect was associated to a change of the magnetization reversal

dynamics due to the variation of the out of plane component of the magnetic anisotropy by substrate-induced strains detected in the structural characterization of the samples.

Data availability statement

All data that support the findings of this study are included within the article (and any supplementary files).

Acknowledgment

Authors thanks the financial support of FONCYT PICT 0867-2016, PICT 02781-2019 and the European Commission through the Horizon H2020 funding by H2020-MSCA-RISE-2016–Project No. 734187 –SPICOLST. Beamtime was Granted on the XRD2 beamline by the LNLS. C G acknowledges the financial support received by ANID FONDECYT/REGULAR 1201102, ANID PIA/APOYO AFB180002 and ANID FONDEQUIP EQM140161.

ORCID iDs

A Román  <https://orcid.org/0000-0002-7979-2076>
 A Lopez Pedrosa  <https://orcid.org/0000-0002-5004-2343>
 A Butera  <https://orcid.org/0000-0003-2466-8972>
 M H Aguirre  <https://orcid.org/0000-0002-1296-4793>
 M Medeiros Soares  <https://orcid.org/0000-0001-8128-7901>
 C Garcia  <https://orcid.org/0000-0002-4578-5396>
 L B Steren  <https://orcid.org/0000-0003-2224-9272>

References

- [1] Mathews M, Houwman E P, Boschker H, Rijnders G and Blank D H 2010 *J. Appl. Phys.* **107** 013904
- [2] Yoo Y, Kläui M, Vaz C, Heyderman L and Bland J 2003 *Appl. Phys. Lett.* **82** 2470–2
- [3] Wang J, Sepelri-Amin H, Takahashi Y, Okamoto S, Kasai S, Kim J, Schrefl T and Hono K 2016 *Acta Mater.* **111** 47–55
- [4] Hauet T et al 2014 *Phys. Rev. B* **89** 174421
- [5] Garnier L C, Marangolo M, Eddrief M, Bisero D, Fin S, Casoli F, Pini M G, Rettori A and Tacchi S 2020 *J. Phys. Mater.* **3** 024001
- [6] Parkin S and Yang S H 2015 *Nat. Nanotechnol.* **10** 195–8
- [7] Hierro-Rodríguez A et al 2017 *Appl. Phys. Lett.* **110** 262402
- [8] Hierro-Rodríguez A, Quirós C, Sorrentino A, Blanco-Roldán C, Alvarez-Prado L M, Martín J I, Alameda J, Pereiro E, Vélez M and Ferrer S 2017 *Phys. Rev. B* **95** 014430
- [9] Sadovnikov A V, Odintsov S A, Beginin E N, Sheshukova S E, Sharaevskii Y P and Nikitov S A 2017 *Phys. Rev. B* **96** 144428
- [10] Liu C et al 2019 *Nat. Nanotechnol.* **14** 691–7
- [11] Spain R and Fuller H 1966 *J. Appl. Phys.* **37** 953–9
- [12] Tee Soh W, Phuoc N N, Tan C and Ong C 2013 *J. Appl. Phys.* **114** 053908
- [13] Wei J, Zhu Z, Song C, Feng H, Jing P, Wang X, Liu Q and Wang J 2016 *J. Phys. D: Appl. Phys.* **49** 265002
- [14] Fin S et al 2015 *Phys. Rev. B* **92** 224411
- [15] Camara I S, Tacchi S, Garnier L C, Eddrief M, Fortuna F, Carlotti G and Marangolo M 2017 *J. Phys.: Condens. Matter* **29** 465803
- [16] Álvarez N R, Montalbetti M V, Gomez J E, Riffo A M, Álvarez M V, Goovaerts E and Butera A 2015 *J. Phys. D: Appl. Phys.* **48** 405003
- [17] Guzmán J M, Álvarez N, Salva H R, Mansilla M V, Gómez J and Butera A 2013 *J. Magn. Magn. Mater.* **347** 61–67
- [18] Sallica Leva E, Valente R C, Tabares F M, Mansilla M V, Roshdestwensky S and Butera A 2010 *Phys. Rev. B* **82** 144410
- [19] Tacchi S et al 2014 *Phys. Rev. B* **89** 024411
- [20] Spada F, Parker F, Platt C and Howard J 2003 *J. Appl. Phys.* **94** 5123–34
- [21] Toney M F, Lee W Y, Hedstrom J A and Kellock A 2003 *J. Appl. Phys.* **93** 9902–7
- [22] Lyubina J V 2007 *Nanocrystalline Fe-Pt Alloys: Phase Transformations, Structure and Magnetism* (Cuvillier Verlag)
- [23] Bayliss P 1990 *Can. Mineral.* **28** 751–5
- [24] Yuasa S, Miyajima H and Otani Y 1994 *J. Phys. Soc. Japan* **63** 3129–44
- [25] Soares M M, Tolentino H C N, De Santis M, Ramos A Y and Cezar J C 2011 *J. Appl. Phys.* **109** 07D725
- [26] Soares M M, Lamirand A D, Ramos A Y, De Santis M and Tolentino H C 2014 *Phys. Rev. B* **90** 214403
- [27] Hai N, Dempsey N, Veron M, Verdier M and Givord D 2003 *J. Magn. Magn. Mater.* **257** 139–45
- [28] Buschow K V, Van Engen P and Jongebreur R 1983 *J. Magn. Magn. Mater.* **38** 1–22
- [29] White R L 2000 *J. Magn. Magn. Mater.* **209** 1–5
- [30] Coffey K R, Thomson T and Thiele J U 2002 *J. Appl. Phys.* **92** 4553–9
- [31] Oh D and Park J K 2005 *J. Appl. Phys.* **97** 10N105
- [32] Stoner E C and Wohlfarth E 1948 *Phil. Trans. R. Soc. A* **240** 599–642
- [33] Kondorsky E 1940 *J. Phys. USSR* **2** 161–81
- [34] Byun C, Sivertsen J and Judy J 1986 *IEEE Trans. Magn.* **22** 1155–7
- [35] Shtrikman S and Treves D 1959 *J. Phys. Radium* **20** 286–9
- [36] Fisher R and Khan M R 1990 *IEEE Trans. Magn.* **26** 1626–8
- [37] Jeong S, Hsu Y N, Laughlin D E and McHenry M E 2000 *IEEE Trans. Magn.* **36** 2336–8
- [38] Suponev N, Grechishkin R, Lyakhova M and Pushkar Y E 1996 *J. Magn. Magn. Mater.* **157** 376–7
- [39] Vansteenkiste A, Leliaert J, Dvornik M, Helsen M, Garcia-Sanchez F and Van Waeyenberge B 2014 *AIP Adv.* **4** 107133
- [40] Leliaert J, Van de Wiele B, Vansteenkiste A, Laurson L, Durin G, Dupré L and Van Waeyenberge B 2014 *J. Appl. Phys.* **115** 233903
- [41] Leliaert J, Mulkers J, De Clercq J, Coene A, Dvornik M and Van Waeyenberge B 2017 *AIP Adv.* **7** 125010
- [42] Exl L, Bance S, Reichel F, Schrefl T, Peter Stimming H and Mauser N J 2014 *J. Appl. Phys.* **115** 17D118
- [43] Okamoto S, Kikuchi N, Kitakami O, Miyazaki T, Shimada Y and Fukamichi K 2002 *Phys. Rev. B* **66** 024413
- [44] Kanazawa H, Lauhoff G and Suzuki T 2000 *J. Appl. Phys.* **87** 6143–5
- [45] Weller D, Parker G, Mosendz O, Lyberatos A, Mitin D, Safonova N Y and Albrecht M 2016 *J. Vac. Sci. Technol. B* **34** 060801
- [46] Birkholz M and Genzel C 2006 *Thin Film Analysis by X-ray Scattering* (New York: Wiley)
- [47] Ramos C, Brigneti E V, Gómez J and Butera A 2009 *Physica B* **404** 2784–6
- [48] Hsiao S, Yuan F, Chang H, Huang H, Chen S and Lee H 2009 *Appl. Phys. Lett.* **94** 232505
- [49] Birkholz M 2006 *Thin Film Analysis by X-ray Scattering* (New York: Wiley)
- [50] Takahashi Y, Seki T, Hono K, Shima T and Takanashi K 2004 *J. Appl. Phys.* **96** 475–81
- [51] Takahashi Y, Koyama T, Ohnuma M, Ohkubo T and Hono K 2004 *J. Appl. Phys.* **95** 2690–6
- [52] Takahashi Y, Ohkubo T, Ohnuma M and Hono K 2003 *J. Appl. Phys.* **93** 7166–8
- [53] Murayama Y 1966 *J. Phys. Soc. Japan* **21** 2253–66
- [54] Johnson M, Bloemen P, Den Broeder F and De Vries J 1996 *Rep. Prog. Phys.* **59** 1409
- [55] Bisio F, Moroni R, Buatier de Mongeot F, Canepa M and Matterna L 2006 *Appl. Phys. Lett.* **89** 052507
- [56] Alvarez-Prado L M, Pérez G T, Morales R, Salas F H and Alameda J M 1997 *Phys. Rev. B* **56** 3306
- [57] Hughes G F 1983 *J. Appl. Phys.* **54** 5306–13
- [58] Coey J M 2010 *Magnetism and Magnetic Materials* (Cambridge: Cambridge University Press)
- [59] Janssen G 2007 *Thin Solid Films* **515** 6654–64
- [60] Rasmussen P, Rui X and Shield J E 2005 *Appl. Phys. Lett.* **86** 191915
- [61] Leiva L, Torres J A, Gómez J, Rodríguez D V, Milano J and Butera A 2022 *J. Magn. Magn. Mater.* **544** 168619
- [62] Ruffoni M, Ndao C, Dempsey N, Pascarelli S and Givord D 2008 The local atomic-scale joule magnetostriction of FePt *Joint European Magnetics Symp. 2008 (Trinity College, Dublin, Ireland, 14 September 2008)* (available at: <http://hdl.handle.net/10044/1/6014>)